The impact of apicobasal ridges on dental load-bearing capacity in aquatic-feeding predatory amniotes

Ailie S. MacKenzie[1,2] 🆔, Glenn A. Brock[1] and Matthew R. McCurry[2,3,4]

[1]School of Natural Sciences, Macquarie University, New South Wales 2109, Australia.
[2]Australian Museum Research Institute, 1 William Street, Sydney, New South Wales 2010, Australia.
[3]Earth and Sustainability Science Research Centre, School of Biological, Earth and Environmental Sciences (BEES), University of New South Wales, Kensington, New South Wales 2052, Australia.
[4]Paleobiology, National Museum of Natural History, Smithsonian Institution, Washington, D.C. 20560, U.S.A.

Non-technical Summary

Complex enamel ridges have evolved multiple times on the teeth of unrelated aquatic predators, including extinct marine reptiles, toothed whales, crocodilians, and aquatic-feeding dinosaurs. Their appearance in such a wide range of groups suggests that they are a specialized structure adapted to perform specific functions in the capture and/or processing of prey, although these functions are unknown. This study used computer modeling to apply bite force simulations to a set of digital tooth models in order to identify whether the ridges strengthened the tooth. These models enabled us to visualize how bite force stress is distributed around smooth teeth compared with ridged teeth, including a range of ridge types. Our results suggested that the ridges do not strengthen the tooth crown overall, indicating that they may instead serve another role in prey handling.

Abstract

Apicobasal ridges are longitudinal ridges of enamel that are particularly common in several clades of aquatic-feeding predatory amniotes, including Plesiosauria, Ichthyosauria, Mosasauridae, Crocodylia, and Spinosauridae, as well as some early members of Cetacea. Although the repeated evolution of these dental ridges in unrelated clades suggests an adaptive benefit, their primary function in feeding is debated. Hypothesized functions range from increasing tooth strength to improving prey puncture or removal efficiency, but these have never been quantitatively tested. This study utilizes finite element analysis (FEA) to assess the impact of apicobasal ridges upon tooth crown strength in aquatic-feeding amniotes. Drawing on morphometric data from fossilized tooth crowns, a set of digital models was constructed to calculate the performance of smooth and ridged tooth variants under simulated bite force loadings. The similarities in overall stress distribution patterns across models of the same tooth shape, regardless of the presence or morphology of ridges, indicate that apicobasal ridges have little impact on stress reduction within the tooth crown. Ultimately, these findings suggest that apicobasal ridges have a minimal role in improving crown strength and form a framework for future research into the remaining hypotheses.

Introduction

Geological time has borne witness to many reinvasions of the aquatic environment by lineages of terrestrial tetrapods (Fish 2016). These reinvasions were dependent upon a variety of evolutionary shifts in morphological and behavioral traits (Fish 2016; Houssaye and Fish 2016). The return to aquatic environments placed immense selective pressure on the terrestrial Bauplan, resulting in widespread convergence of morphological traits between secondarily aquatic tetrapods (Howell 1930; Braun and Reif 1985; Thewissen and Nummela 2008; Houssaye and Fish 2016). Although recent research into aquatic-feeding predators has focused on the dietary significance of tooth shape (Lukeneder and Zverkov 2020; Sulcova et al. 2020; Fischer et al. 2022), little is known about the function of crown surface morphology. This gap is particularly evident in the case of apicobasal ridges, longitudinal enamel ridges present in several clades of secondarily aquatic amniotes (McCurry et al. 2019) (Fig. 1). The structural makeup of these ridges varies between taxa; cross-sectional analysis by McCurry et al. (2019) demonstrates that in plesiosaurs, the ridges do not extend into the dentine, resulting in thicker enamel at their peaks, which may be due to differential growth rates between enamel types (Sander 1999, 2000). In other clades, including spinosaurids, odontocetes, and crocodilians, the intersection between dentine and enamel extends parallel to the outer surface of the ridges (McCurry et al. 2019). In ichthyosaurs, the ridges mirror an internal dentine folding known as plicidentine, which begins within the crown and extends toward the root
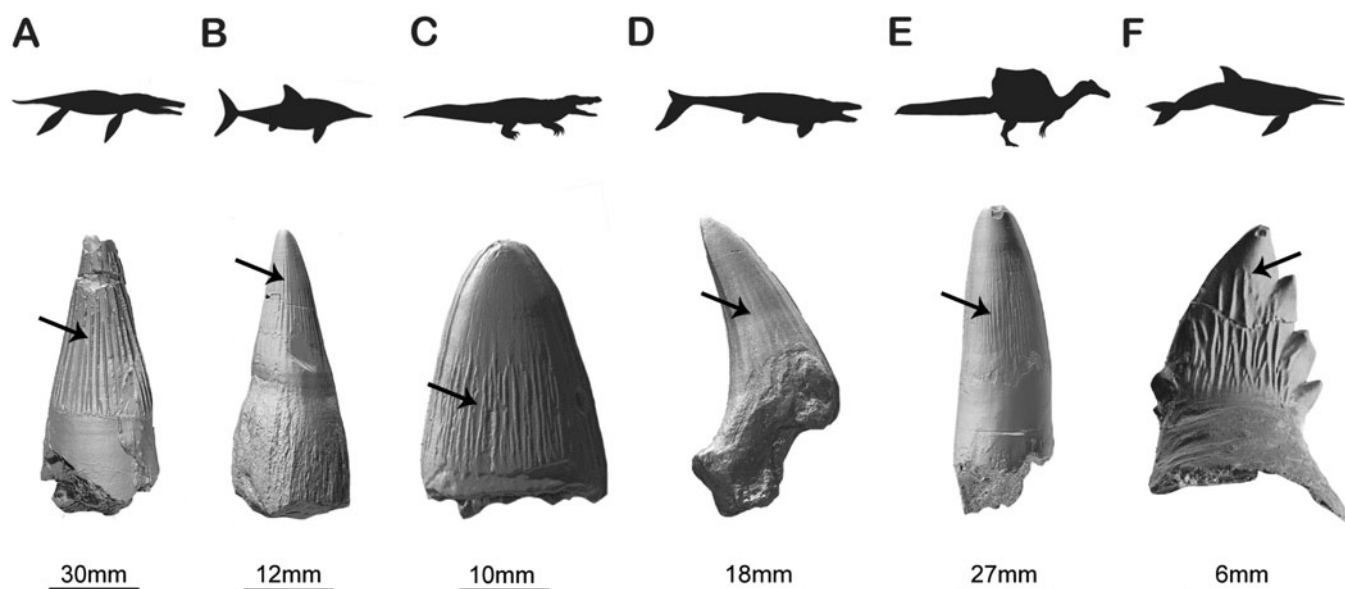
Figure 1. Bauplan silhouettes and tooth faces bearing apicobasal ridges from members of six major aquatic-feeding amniote clades. A, *Pliosaurus brachydeirus* (Plesiosauria) (ROM 5596). B, *Pervushovisaurus campylodon* (Ichthyosauria) (ROM 00334 A). C, *Deinosuchus rugosus* (Crocodylia) (USNM 5351). D, *Tylosaurus proriger* (Mosasauridae) (USNM 3885). E, *Spinosaurus* sp. (Spinosauridae) (ROM 64659). F, *Aetiocetus cotylalveus* (Odontoceti) (USNM 25210 Tooth 1). Arrows indicate apicobasal ridges.

(Maxwell et al. 2012; McCurry et al. 2019). These disparate structural morphotypes support a convergent result, implying distinct amelogenetic pathways to an analogous trait (Sander 1999; McCurry et al. 2019).

Apicobasal ridge morphologies vary in shape, size, and arrangement. The abundance of morphological variation, even within some lower-ranked taxa, suggests that—like crown shape (Massare 1987)—ridge morphologies are related to diet rather than clade, although species specificity does occur (Benson et al. 2013; Zverkov et al. 2018). One example of this species specificity is the common characterization of plesiosaur teeth by widely spaced, distinct ridges on a smooth surface, with an often trihedral tooth shape (Benson et al. 2013; Zverkov et al. 2018).

Some specimens with ridges around the entire crown circumference, such as some Late Cretaceous material previously attributed to *Polyptychodon*, display density that differs between tooth faces, with lingual ridges clustering more closely than buccal ridges (Madzia 2016). In taxa with trihedral or subtrihedral crown cross sections, ridges may be present on only one or two of the faces, typically excluding the buccal face (Fischer et al. 2015). These taxa also often trend toward an increased clustering of ridges on the lingual surface (Taylor 1992; Buffetaut 2013; Richter et al. 2013).

The ridges themselves can be high or low relief, varying within individual teeth as well as between species, but remain visually distinct from smooth enamel (Buffetaut 2013). Coverage of the apicobasal length is also variable; across taxa, ridges taper off or anastomose anywhere from a few millimeters above the base to directly below the apex (Massare 1987; Young et al. 2014; Madzia 2016).

The strength hypothesis is among the most frequently cited hypotheses aiming to explain the function of apicobasal ridges in aquatic feeding strategies. This hypothesis focuses upon the potential for the ridges to strengthen the tooth crown (Preuschoft et al. 1974; Vaeth et al. 1985; Young and Kardong 1996; Schulp 2005; Young et al. 2014; Zverkov et al. 2018), possibly by channeling pressure toward its base and the "valleys" between ridges (Preuschoft et al. 1974; Rieppel and Labhardt 1979; Sander 1999) or by increasing the second moment of area (I), an engineering principle that quantifies the rigidity of a shape and would enable the ridges to act comparably to corrugations in a metal sheet by increasing the load-bearing surface area (Khalid et al., 2004). It should be noted, however, that the latter comparison is somewhat confounded by the addition of dentine below the enamel ridges, increasing I, while metal sheets generally bear no additional material below their corrugations. As the strength hypothesis is only one of several plausible hypotheses, the remainder of which include improving grip on slippery prey and enhancing puncture efficiency (McCurry et al. 2019; Crofts et al. 2020), testing is required to better understand the physical capabilities of the ridges and any strength advantages they may have conferred.

Here we aim to assess the impact of apicobasal ridges on the ability of the tooth crown to resist various loading conditions, through the application of finite element analysis (FEA). We compare von Mises stress responses across a range of typical apicobasal ridge morphologies, analyzing the influence of ridge shape, size, and arrangement on crown strength. Furthermore, we use comparative morphometrics to evaluate morphological variation in apicobasal ridges and determine whether morphologies are clustered by phylogeny. Although ridge morphology is relatively well documented in plesiosaurs (Benson et al. 2013; Fischer et al. 2015; Madzia 2016; Zverkov et al. 2018), our knowledge of trends in other taxa, such as odontocetes, ichthyosaurs, and mosasaurs, is currently limited and may be expanded through this study.

Materials and Methods

Specimen Selection and Imaging

Forty-eight individual tooth specimens were selected to represent six major clades of aquatic-feeding amniotes (Plesiosauria, Ichthyosauria, Crocodylia, Mosasauridae, Spinosauridae, and Odontoceti) (Appendix 1). Specimen selection was informed primarily by preservation, excluding worn and damaged specimens

for which a cross section could not be measured. As only one set of specimens (ROM 12809 Tooth A–F) was originally found in partial articulation, all specimens in the dataset have been treated as isolated teeth. We were unable to assign positions within the jaw for each tooth due to the prevalence of homodont dentition in marine reptiles (Ciampaglio et al. 2005). While position along the toothrow affects the amount of force experienced by a crown (Bourke et al. 2008; Cohen et al. 2020), it is less likely to affect potential directions of force (lateral and vertical). As this study compares responses to directional force, jaw position is unlikely to greatly affect the results. Specimens were instead selected to portray a variety of ridge and crown morphologies.

The specimens were drawn from the collections of four museums. High-resolution microcomputed tomography and neutron imaging were utilized by previous researchers to digitize the specimens (McCurry et al. 2019). This process was completed using either Nikon Metrology's combined 225/450 kV microfocus X-ray and computed tomography (CT) walk-in vault system at Chesapeake Testing in Belcamp, Md., U.S.A., or the DINGO neutron beamline at Australia's Nuclear Science and Technology Organisation (ANSTO) in Lucas Heights, NSW, Australia (McCurry et al. 2019). The teeth were then digitally isolated from the CT scan and exported as three-dimensional surface models in STL (standard triangular language) format by previous researchers (McCurry et al. 2019).

Institutional Abbreviations. **KKF**: Kronosaurus Korner, Richmond, QLD, Australia; **NHM**: Natural History Museum, London, U.K.; **ROM**: Royal Ontario Museum, Toronto, ONT, Canada; and **USNM**: National Museum of Natural History, Smithsonian Institution, Washington, D.C., U.S.A.

Data Collection

The three-dimensional models were orientated within a Cartesian coordinate system and measured in Rhino v. 6 (McNeel 2019).

Crown height was recorded from the enamel dentine junction to the apex of the crown (Fig. 2, Appendix 2). Where the apex was incomplete, measurement concluded at the highest point of the crown to avoid overestimation of crown height, although we acknowledge this would also result in a slight underestimation within some specimens. Crown width was recorded at the widest point of the crown for both the labiolingual and mesiodistal orientations (Fig. 2, Appendix 2). For mold fossil specimens that lacked a three-dimensional crown, width was recorded only for the visible orientation.

Ridge height and width measurements were taken for 10 ridges per tooth across a lateral cross section of the crown at 50% of its height (Appendix 3). The apicobasal span of the ridges was recorded as a percentage of the total crown height (Appendix 2). If a cross section bore more than 10 ridges, 10 were randomly selected for data collection. If fewer than 10 ridges were identified, the specimen was excluded from the ridge measurement section of the study. The overall count of ridges around the circumference of the cross section were recorded, regardless of whether the tooth was included in the measurement section, to gain a holistic understanding of ridge count across all taxa. Carinae were not classified as apicobasal ridges for the purposes of this study, as they are commonly accepted to be separate structures differing in abundance and relief (Young et al. 2014; Hendrickx et al. 2015; McCurry et al. 2019). All linear measurements were log transformed in R v. 4.0.4 (R Core Team 2021) to conform to a normal distribution and to visualize morphological differences between specimens that vary considerably in the analyzed traits.

Analysis of Ridge Morphology

Linear Regression Models. A range of morphological variables measured on the specimens were fit to linear regression models to investigate the dental diversity of aquatic-feeding amniotes and identify taxon-specific traits. The use of linear regression models allows an evaluation of variance in all relationships of potential interest and provides insight into isometry or allometry

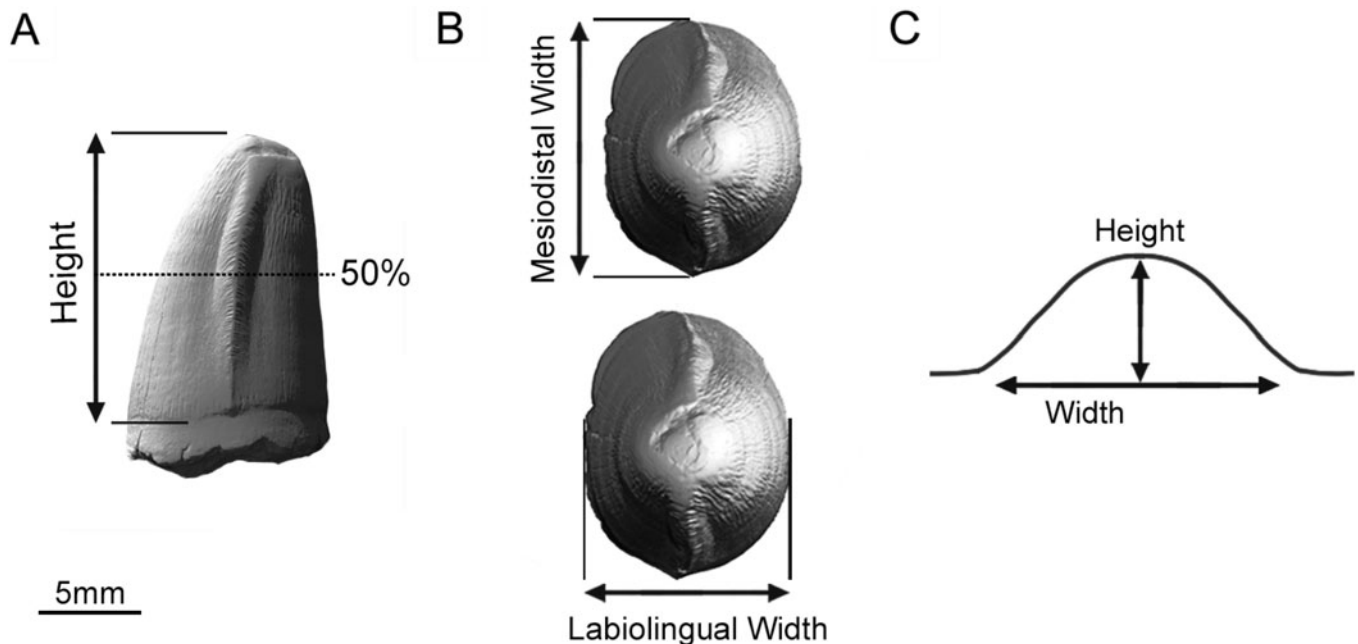

Figure 2. Standard measurements recorded for fossilized tooth specimens. A, Crown height and position of lateral cross section at 50% of the height (dotted line). B, Crown width measurements (both mesiodistal and labiolingual). C, Apicobasal ridge height and apicobasal ridge width within a cross-section outline (not to scale). Demonstrated on a *Bottosaurus* sp. tooth crown (USNM 508536).
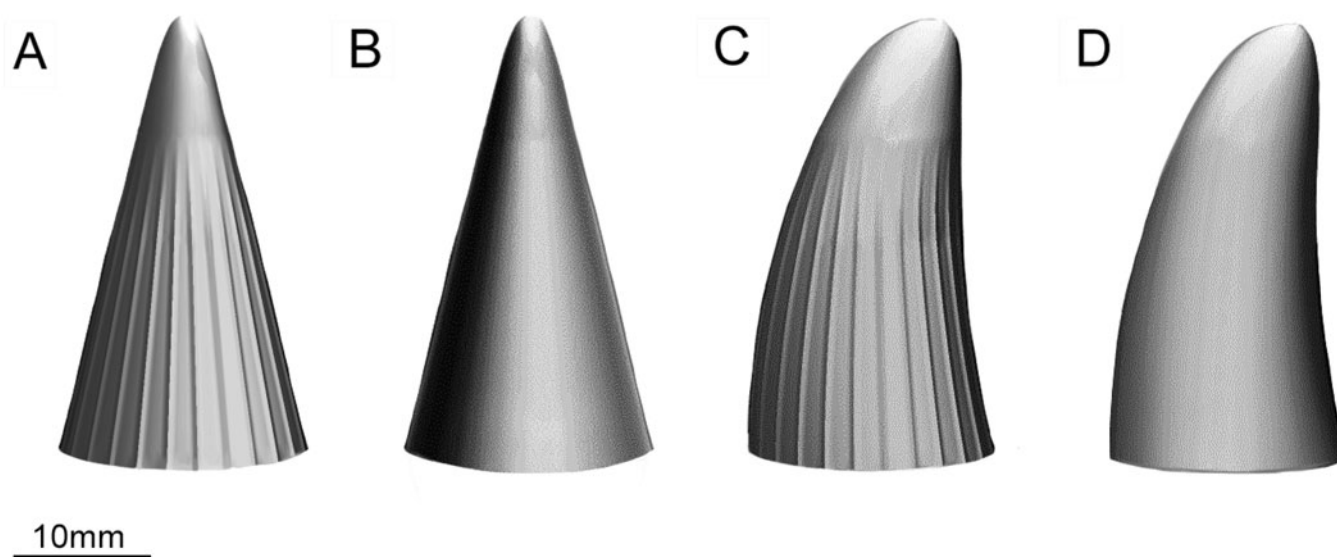
Figure 3. Comparison between select examples of ridged and smooth digital tooth models. A, Average Ridges model (ridge width = 0.663 mm, ridge height = 0.136 mm). B, No Ridges (Conical) model. C, Symmetrical Ridges model. D, No Ridges (Recurved) model. All models are in mesial view.

within the scaling mechanics of the ridges. The compared variables included relative apicobasal ridge height and width, crown height and width, and ridge count. Relative ridge measurements were included to ensure the exclusion of size bias and were calculated by dividing each tooth's average ridge height or width by the crown height or width respectively. The labiolingual and mesiodistal crown width measurements were averaged to provide a representative singular width for the regression models. All models utilizing count data were analyzed using a generalized linear model with a quasi-Poisson distribution to accommodate this type of data and variance dispersion. All regression models were conducted and plotted in R v. 4.0.4 (R Core Team 2021).

Taxonomic Variance in Ridge Morphology. To determine any significant differences between the average ridge data of the six aquatic-feeding amniote groups examined in this study, univariate Kruskal-Wallis tests were performed in R v. 4.0.4 (R Core Team 2021). These variance tests were run on data for relative crown height, relative crown width, and ridge count across all six groups. All R scripts are available in the Supplementary Material.

FEA

FEA is a numerical technique enabling the digital simulation of directional force across mechanical components of complex structures (Clough 1990; Dumont et al. 2005). In FEA software, the visualization of stress and strain is directed by the application of load cases and constraints in contextually relevant positions across a model (Dumont et al. 2005). Our study conducted FEA upon digital tooth crown models to determine the impact of apicobasal ridges upon overall crown strength. These tests utilized von Mises stress distributions to compare model performance under the simulation of various loading conditions. Von Mises stress is often incorporated into biological model analyses to establish potential failure points under a ductile model of fracture or a model in which deformation precedes breakage (Dumont et al. 2009; Rajabizadeh et al. 2021). Although we acknowledge that enamel and dentine conform to a brittle pattern

of fracture, thus making von Mises stress unsuitable to predict their failure points, it does offer a thorough visualization of stress distribution for these materials (Neves et al. 2015) and is frequently used as such in biomechanical analyses of teeth (Whitenack et al. 2011; Palci et al. 2021; Rajabizadeh et al. 2021; Pollock et al. 2022). Thus, to enable a comparison between our results and similar biological studies, we have utilized von Mises stress to visualize our stress distribution. All FEA was completed using Strand7 v. 2.4.6.*

Model Creation. The tooth crown and apicobasal ridge data were used as a foundation for the construction of a digital set of seven three-dimensional tooth crown models in Rhino v. 6 (Fig. 3; see Supplementary Material). To reflect the scope of tooth crown morphologies within the dataset, the models were based on two of the most widespread crown shapes in aquatic-feeding dentition (conical and recurved). Common variations in ridge size and shape were re-created on conical models, while variations in ridge arrangement were re-created on recurved models to replicate the range documented in recurved teeth (Taylor 1992; Buffetaut 2013; Richter et al. 2013).

The Average Ridges model represents the average ridge measurements, the height and width of which were applied to all models except the Large Ridges model, which instead bears both wider and taller ridges matching the maximum recorded dimensions. The Rounded Ridges model exemplifies ridges with a rounded cross section. The Lingual Clustering model bears ridges only on the recurved lingual face, while the Symmetrical Ridges model represents recurved teeth with ridges around the entire circumference.

Although many fossil specimens have ridges of varying lengths along the crown, all ridges in our models ended at 72% of the crown height (the proportional average) to ensure standardization. Control models without ridges were created for both tooth shapes to enable a comparison between identical teeth with and

*https://www.strand7.com.

without ridges ([Fig. 3]). All models were designed to fit the average crown height and width to eliminate size bias. Although ridge shape can manifest as triangular or rounded in cross section, depending on taxon (McCurry et al. [2019]), triangular ridges were used as the default ridge shape due to the challenges in modeling rounded ridges.

Meshing and Scaling. Each model was imported as an STL surface mesh into Strand7 v. 2.4.6. The models were cleaned and automatically remeshed to a new surface mesh of three-noded triangular plate elements. This methodology reduces warping and allows the accurate application of geometry in complex areas (Dumont et al. [2005]). The refined surface mesh was then used as a base to create a solid mesh of four-noded tetrahedral elements, and the plate elements were deleted upon completion. All models were scaled to the same surface area, as previous research indicates that scaling to surface area will return a consistent stress energy across models of different sizes and surface areas (Dumont et al. [2009]).

Material Properties. As dentine comprises the bulk of the crown mass and aids in the dissipation of force, the mechanical properties of dentine are applied to the mesh, in line with previous studies (Jansen van Vuuren et al. [2016]). These parameters were utilized for both the Young's modulus ($E = 18{,}000$ MPa) and Poisson's ratio ($\nu = 0.31$) (Bensonne et al. [2014]). It is possible that the applied properties do not accurately represent the enamel structure of the crown, due to the differing compressive and tensile strength of enamel and dentine (Milewski [2005]). This is exacerbated by the taxonomic differences in the thickness and arrangement of enamel, from the thickened ridges in plesiosaurs to the plicidentine of ichthyosaurs (McCurry et al. [2019]), as these compositional disparities may have biomechanical effects due to the higher force resistance of dentine and higher wear resistance in enamel (Chun et al. [2014]). Although a recent study found that the material properties of dentine and enamel did not differ enough to affect von Mises stress distributions in reptile mandibles when enamel thickness was altered (Herbst et al. [2021]), it is possible that an effect would have been present in a smaller area localized only upon the tooth. While the internal homogeneity of our models is, as such, a potential limitation, the study makes an assumption similar to that of Dumont et al. ([2009]) due to the difficulties of accurately representing and modeling the range of internal heterogeneity. Accordingly, we predict that the effects of internal tissue properties would be consistent across all models and treat tooth material properties as homogenous, as in recent literature (Palci et al. [2021]; Pollock et al. [2022]).

Constraints and Load Cases. For the application of realistic constraints, each tooth model was fixed along the degrees of translation and three degrees of rotation by the external nodes across the entire base. This corresponds to the lack of axial displacement that would have been present in the tooth socket.

Load cases were comprised of three primary directional pressures, each simulating a direction of stress that could have been experienced during prey capture, incapacitation, or processing. The primary three load cases were Bite (-40 N per node on the z-axis), Shake (40 N per node on the y-axis), and Pull (-40 N per node on the x-axis) ([Fig. 4]). Two further load cases called Bite and Shake and Bite and Pull combined the prior individual cases to analyze the effects of multiple simultaneous forces. In each of the five load cases, the force loads were applied to the topmost five nodes of each model's apex. While we acknowledge that confining force application to the apex does not encompass a full representation of conditions where the tooth is embedded in prey, it does allow us to model the effects of force applied through a hard surface, such as when the tip of a tooth contacts bone, where any additional strength conferred by ridges would be most relevant.

Bite force data are challenging to attain, even for extant species (Koc et al. [2010]), and are highly correlated to body size (Erickson et al. [2012]), preventing simple estimation for the isolated teeth in this study. Thus, the above loading units were assigned to standardize the applied bite force between models. As this study seeks to compare only the relative performances of models, the standardization of loads without precise bite force data is appropriate to provide an accurate result (Dumont et al. [2009]).

The Bite load case was informed by the expected pressures of a typical vertical bite, involving the forceful closure of the mandible documented in a range of vertebrate predators, including crocodilians (Araújo and Polcyn [2013]). The Shake load case aimed to test the response of teeth to the lateral-shake feeding strategy observed in crocodilians, proposed for the pliosauroid *Rhomaleosaurus* due to similarities with crocodilian cranial morphology (Taylor [1992]). Similarly, the Pull load case was implemented to test the models' response to the backward pulling movements noted in modern crocodilian feeding (Gallagher et al. [2018]). Each of the Bite, Shake, and Pull load cases were applied and assessed on each model separately to obtain an understanding of how the models responded to these pressures individually. However, the inclusion of the Bite and Shake and the Bite and Pull load cases ensured an evaluation of the models' performance under more biologically accurate conditions.

FEA Contour Maps. Each solid mesh was solved as a linear static model, calculating brick stress for both internal and external bricks. The results were displayed as von Mises stress distribution maps, in which concentrations of warm colors indicated high-stress areas, while concentrations of cool colors indicated low-stress areas. Statistical tests of these maps were omitted from this study due to inaccurate conclusions resulting from differences in brick size within and between models.

Results

Crown and Ridge Measurements

From the collected measurements, the average tooth crown height was 32 mm, while the average crown width was calculated as 18.136 mm mesiodistally and 17.917 mm labiolingually. The average absolute apicobasal ridge height and width were calculated as 0.136 mm and 0.663 mm, respectively, and the average ridge extends along approximately 72% of the height of the tooth crown. The average tooth bore 26 apicobasal ridges that reached at least 50% of its height. These measurements were utilized to create the seven theoretical digital tooth models representing the scope of common tooth morphologies in extinct aquatic-feeding amniotes.

Analysis of Ridge Morphology
Linear Regression Models. Regression analysis showed a positive correlation between the average ridge height and crown height ($p < 0.001$, $R^2 = 0.26$) ([Fig. 5A]) and between the average ridge width and crown width ($p < 0.001$, $R^2 = 0.43$) ([Fig. 5B]). The
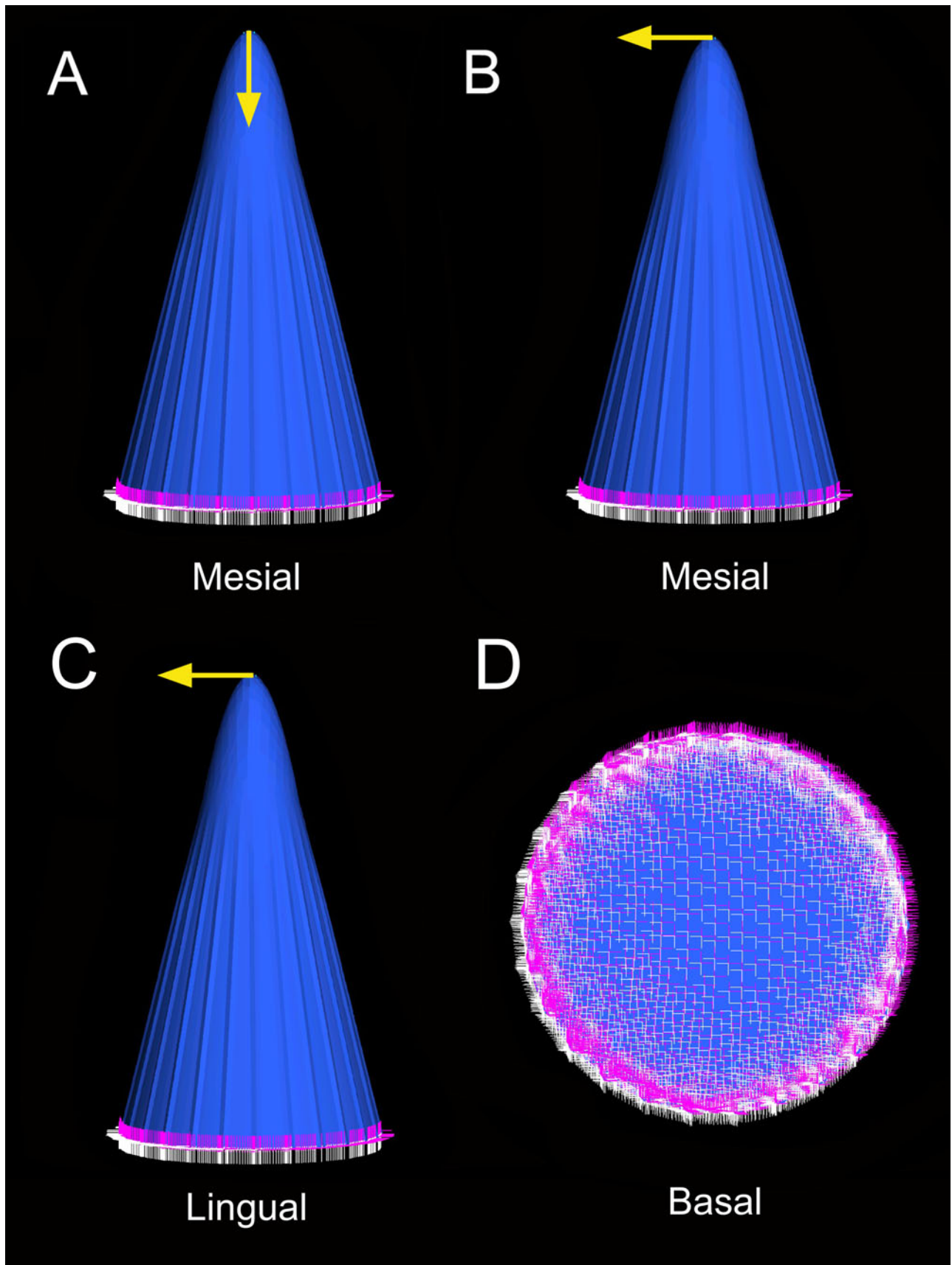
Figure 4. Finite element solid mesh models demonstrating directions of load cases and constraints. All models are Average Ridges model. A, Bite load case from the crown's apex (arrow) and constraint nodes (in pink and white). B, Shake load case from the crown's apex (arrow) and constraint nodes (in pink and white). C, Pull load case from the crown's apex (arrow) and constraint nodes (in pink and white). D, Distribution of constraint nodes across the base (in pink and white).

Figure 5. Linear regression models for apicobasal ridge measurements and tooth crown size in aquatic-feeding amniotes. A, Relative average apicobasal ridge height and crown height. B, Relative average apicobasal ridge width and crown width. Predicted slope of isometry falls outside the visualized datasets.

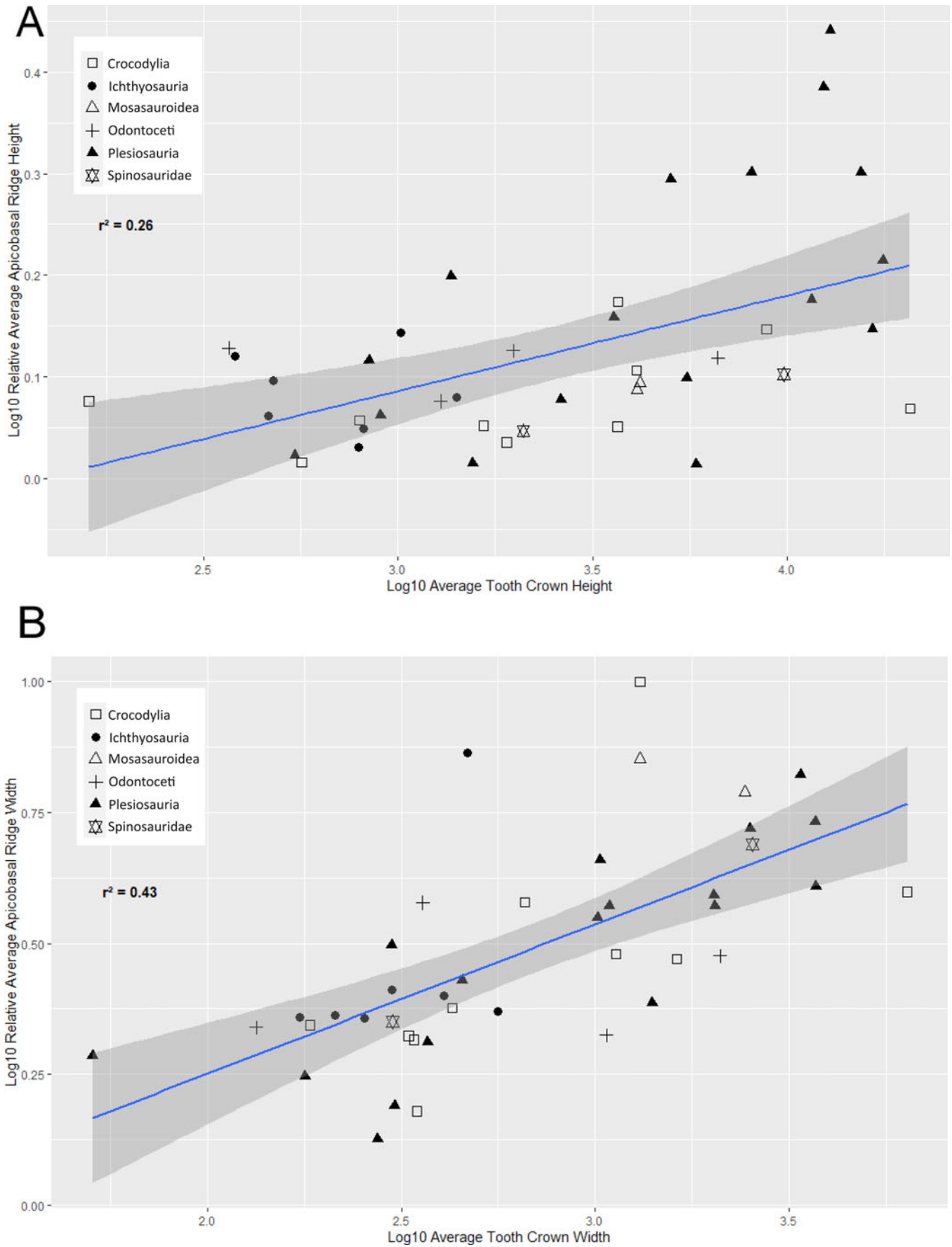regression slope (b) is less than 1 in both the height ($b = 0.094$) and width ($b = 0.285$) regressions. Both averages were calculated from relative measurements.

A negative correlation was found between average relative ridge width and ridge count ($p = 0.003$, $t = -3.114$). However, there was no significant correlation found between relative average ridge height and ridge count ($p = 0.067$, $t = -1.883$).

Taxonomic Variance in Ridge Morphology. The univariate Kruskal-Wallis tests returned no statistically significant difference between the average relative ridge height (chi-squared = 7.897, $p = 0.162$, df = 5) or the average relative ridge width (chi-squared = 6.241, $p = 0.284$, df = 5) of the six taxonomic groups examined within the dataset. Furthermore, no statistically significant difference was found between the average ridge counts for these six groups (chi-squared = 1.691, $p = 0.89$, df = 5).

FEA Contour Maps

The contour maps (Figs. 6–10) show a near-identical distribution of von Mises stress across models of the same tooth shape. Although ridged models show a slightly increased stress distribution within the ridges themselves, the interjacent smooth enamel retains a similar vertical stress gradient across the crown throughout both smooth and ridged models, as well as across all ridge morphologies. As this overall gradient does not differ, it does not appear that the slightly heightened stress in ridges relieves stress within the crown.

Bite Load Case. Under the Bite load case, conical models exhibit high stress concentrations around the apex with an even gradient of stress reduction down the crown (Fig. 6A–D). This longitudinal stress reduction occurs at an equal rate in all conical models.

Some slightly higher stress values appear to be concentrated on the ridges, presenting more prominently around the middle of the Large Ridges model (Fig. 6C).

In recurved models, the higher stress values are located along the lingual face of the crown despite the application of force in the middle of the apex (Fig. 6E–G). This trend occurs in all recurved models under the Bite load case. The overall distribution of stress again appears almost identical across all recurved models, with most of the stress concentrated in the lingual tip of the apex and decreasing toward the buccal base, with a slightly increased stress in the ridges.

Shake Load Case. Under the Shake load case, conical models display a bifurcated stress distribution in which stress is concentrated down the lingual and buccal faces (Fig. 7A–D). Despite the application of force toward the buccal surface, the stress distribution is approximately equal between buccal and lingual faces. Stress reduces gradually from the apex to the base, and the overall stress gradients are similar between ridged and smooth models, although again the ridges present with slightly higher values toward the middle of the tooth.

Recurved models display a similar bifurcation of stress that is spread with a slight skew toward the buccal face due to the recurved shape (Fig. 7E–G). As in the conical models, most of the stress is centered on the apex. The stress gradually reduces toward the base, with a small increase in stress particularly around the lingual edge of the base.

Bite and Shake Load Case. Under the Bite and Shake load case, conical models again demonstrate a bifurcated stress distribution, with stress reducing toward the base, but with a skew toward the buccal face (Fig. 8A–D). This skew aligns with the direction of applied force (toward the apical buccal surface). Again, the ridges

Figure 6. Finite element analysis (FEA) maps for the Bite load case. Models depict von Mises stress distribution for: A, No Ridges (Conical) model; B, Average Ridges model; C, Large Ridges model; D, Rounded Ridges model; E, No Ridges (Recurved) model; F, Symmetrical Ridges model; G, Lingual Clustering model. All models are depicted in occlusal view. High stress is represented by warmer colors, while low stress is represented by cooler colors. Areas of white denote stress values higher than 1.5×10^1. +V indicates vertical load force has been applied on all models.
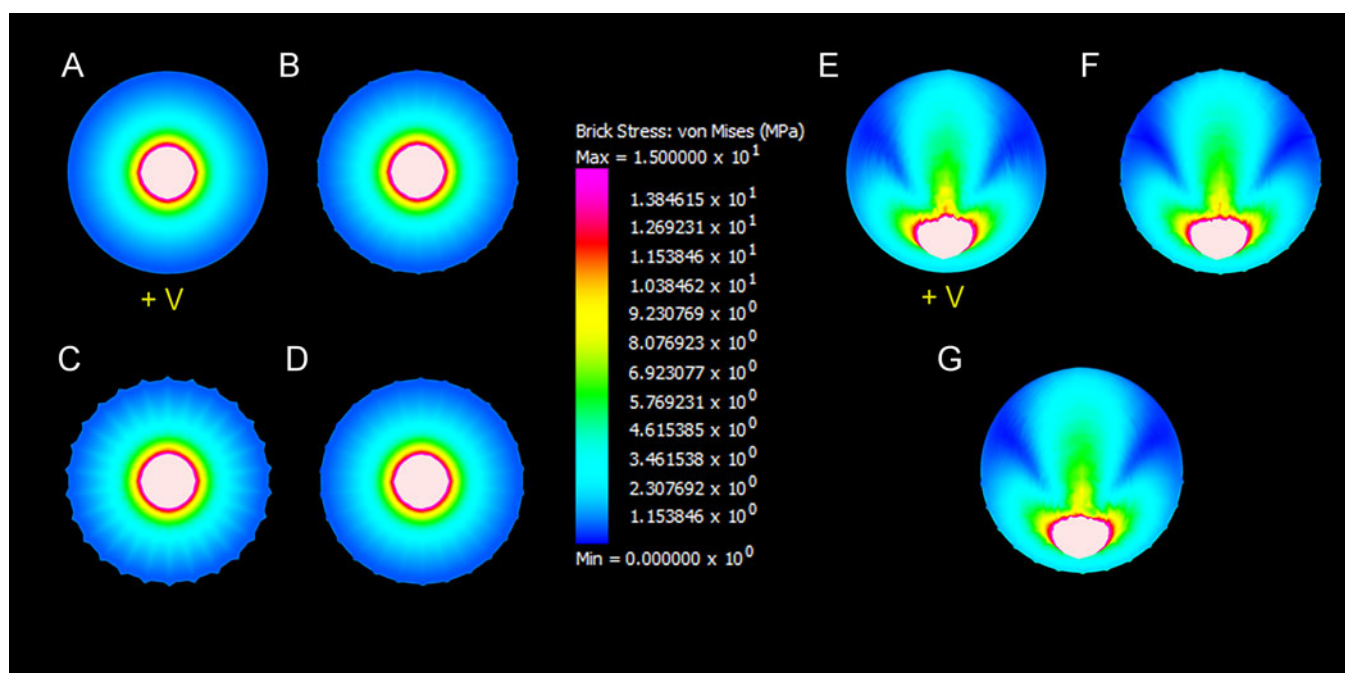
Figure 7. Finite element analysis (FEA) maps for the Shake load case. Models depict von Mises stress distribution for: A, No Ridges (Conical) model; B, Average Ridges model; C, Large Ridges model; D, Rounded Ridges model; E, No Ridges (Recurved) model; F, Symmetrical Ridges model; G, Lingual Clustering model. All models are shown in occlusal view. Areas of white denote stress higher than 2×10^2. Arrows indicate direction of applied load force on all models.

display slightly higher stress, although the overall gradient of distribution is identical between models.

The recurved models all display a bifurcation of stress with a greater buccal skew, again in line with the direction of applied force (Fig. 8E–G). Although the spread of high stress along the crown height is visibly reduced in contrast to the conical models,

it is similar between all of the recurved models, with an extremely slight increase in stress on the lingual ridges.

Pull Load Case. Under the Pull load case, the stress distribution in conical models presents as a reoriented version of the distribution in conical models under the Shake load case, due to the

Figure 8. Finite element analysis (FEA) maps for the Bite and Shake load case. Models depict von Mises stress distribution for: A, No Ridges (Conical) model; B, Average Ridges model; C, Large Ridges model; D, Rounded Ridges model; E, No Ridges (Recurved) model; F, Symmetrical Ridges model; G, Lingual Clustering model. All models are shown in occlusal view. Areas of white denote stress higher than 2×10^2. Arrows indicate direction of applied load force on all models. +V indicates vertical load force has been applied on all models.
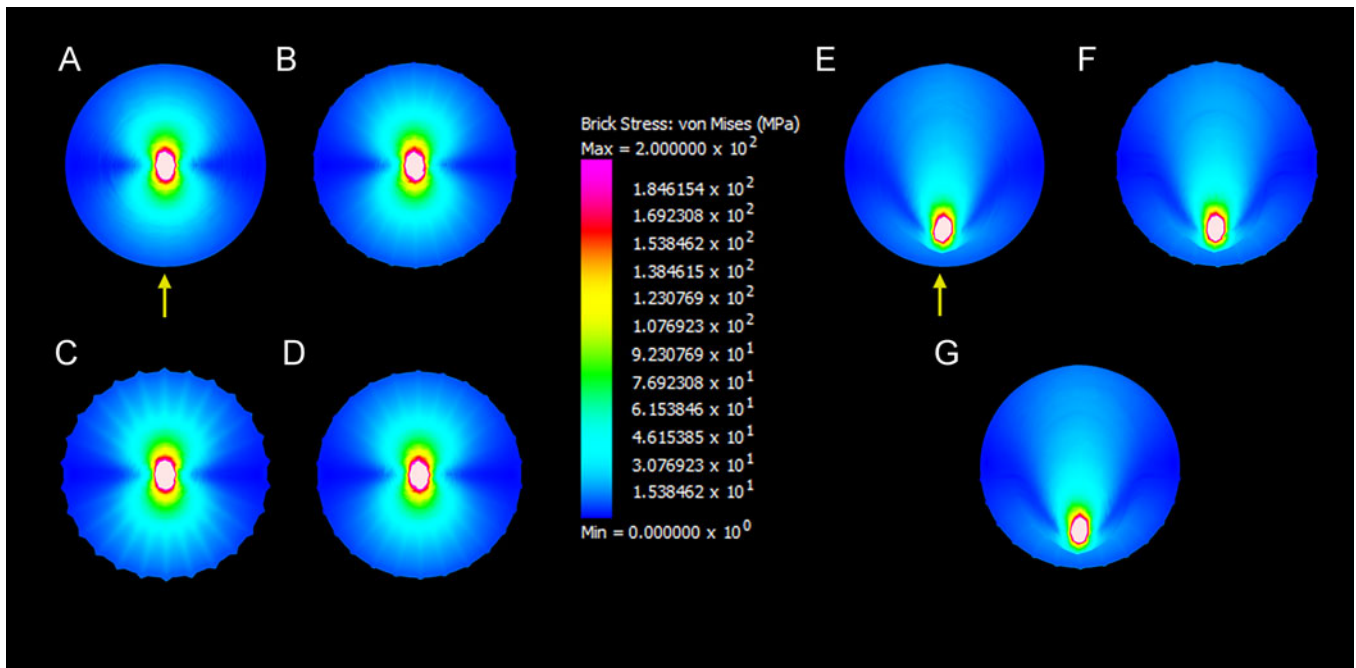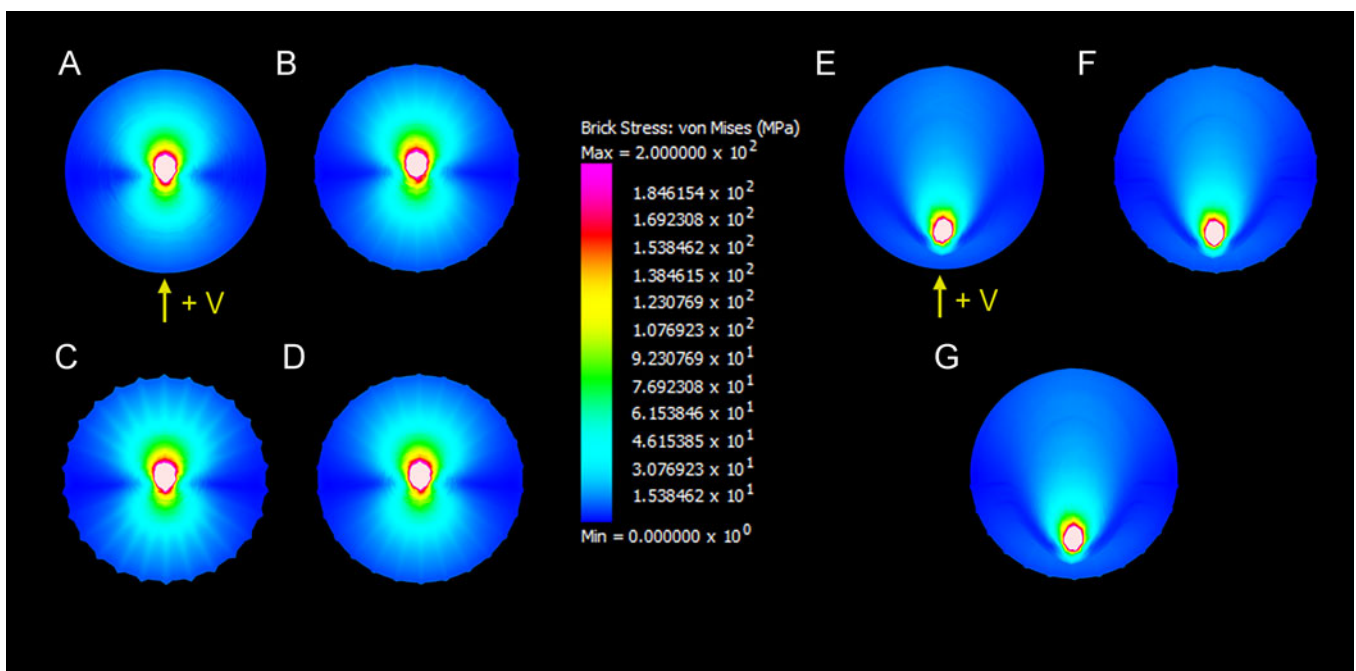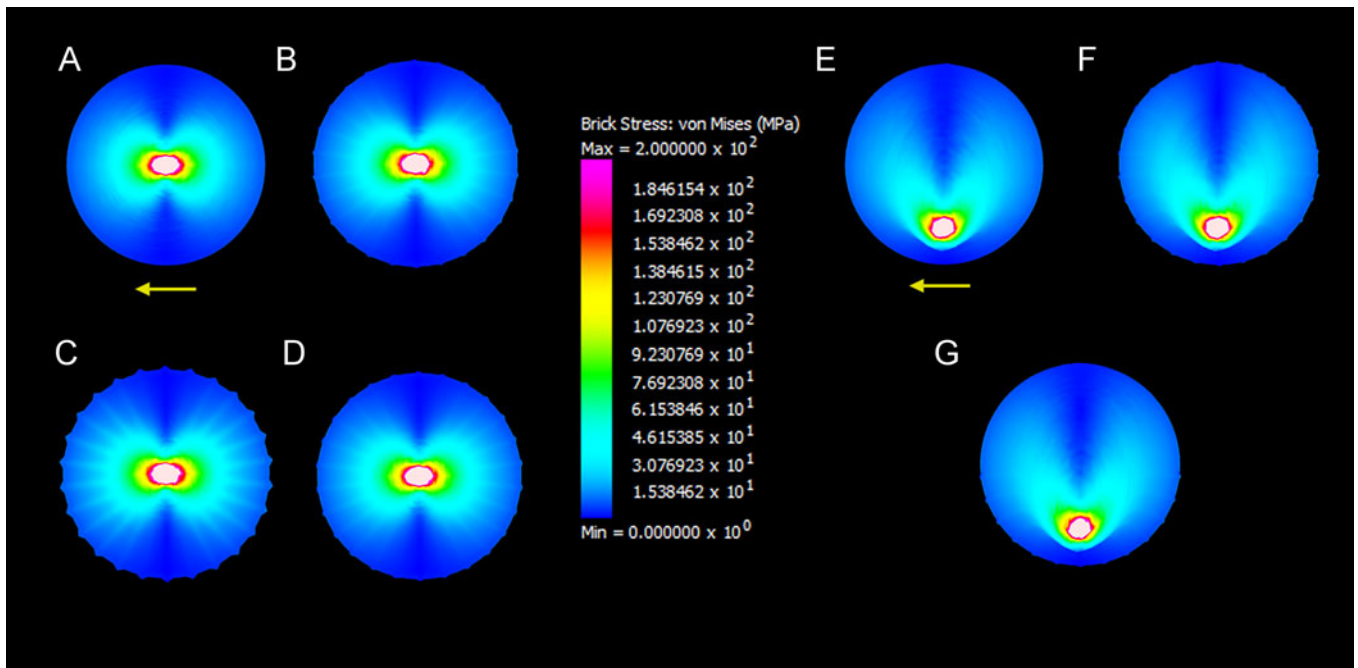
Figure 9. Finite element analysis (FEA) maps for the Pull load case. Models depict von Mises stress distribution for: A, No Ridges (Conical) model; B, Average Ridges model; C, Large Ridges model; D, Rounded Ridges model; E, No Ridges (Recurved) model; F, Symmetrical Ridges model; G, Lingual Clustering model. All models are shown in occlusal view. Areas of white denote stress higher than 2×10^2. Arrows indicate direction of applied load force on all models.

symmetry of the models (Fig. 9A–D). Both ridged and smooth models display a bifurcated distribution in which stress is concentrated equally down the mesial and distal faces, with a slightly increased stress in the ridges.

The bifurcated stress distribution also presents in the recurved models (Fig. 9E–G). As in the conical models, the recurved models show an equal spread of stress down the mesial and distal faces of the crown, with most of the stress centered on the apex. The stress gradually reduces toward the base, although the slight increase in stress in the ridges is more noticeable under this load case than in the Shake case. There are otherwise no substantial differences between the smooth and ridged models within the recurved crown set.

Bite and Pull Load Case. Under the Bite and Pull load case, conical models again demonstrate a bifurcated stress distribution, with stress reducing toward the base, but with a skew in the direction of the applied force (toward the mesial surface) and a slight increase of stress in the ridges (Fig. 10A–D).

The recurved models all display a comparable bifurcation of stress with a mesial skew (Fig. 10E–G). The pattern of slightly higher stress in ridges is more pronounced on the mesial face under the Bite and Pull load case (Fig. 10F–G), in line with the direction of force.

Discussion

Patterns in Ridge Morphology

Linear Regression Models. The positive correlation between apicobasal ridge measurements and tooth crown size indicates a slight trend toward increasing ridge height and width with increasing crown size (Fig. 5). Larger crowns are more likely to develop larger ridges in absolute terms; however, as the regression slope (b) is less than 1 in both models, the relationship between ridge size and crown size is negatively allometric. This suggests that ridges do not develop proportionally to crown size and may be under different selective pressures compared with crown size.

The significant relationship between the relative average ridge width and ridge count ($p < 0.001$, $t = 3.114$) is likely a consequence of spatial constraints. In occupying less space, thinner ridges have a capacity to become densely packed and greater in number, whereas wider ridges limit the available enamel and restrict ridge abundance.

Taxonomic Variance in Ridge Morphology. The lack of statistically significant differences in the average apicobasal ridge measurements between groups suggests an absence of taxon-specific ridge morphologies among the measured characteristics. This supports previous hypotheses claiming that phylogeny bears little to no influence upon ridge morphology (Benson et al. 2013; Zverkov et al. 2018) within the context of ridge height, width, and count.

Our data do provide insight into the breadth of ridge morphologies displayed throughout the studied taxa. Some plesiosaurs have developed low-abundance, high-relief, and lingually clustered ridges (e.g., NHM 2680; NHM 46239 B), while others are characterized by high counts of finer ridges (e.g., ROM 71030; ROM 71033). Crocodilian ridge morphologies are among the most variable, ranging from the high-relief ridges displayed in genera such as *Deinosuchus* (USNM 5351) and *Purussaurus* (USNM 205338) to the rounded, low-relief morphologies present in *Bottosaurus* (USNM 508536). However, one *Bottosaurus* specimen exhibits one of the most distinctive morphologies of the dataset, in its "rippled" and apically anastomosed ridges (USNM 540758). The low, robust crown shape of such teeth has been hypothesized to assist in the crushing of hard-shelled prey items in *Bottosaurus harlani* (Cossette and Brochu 2018),
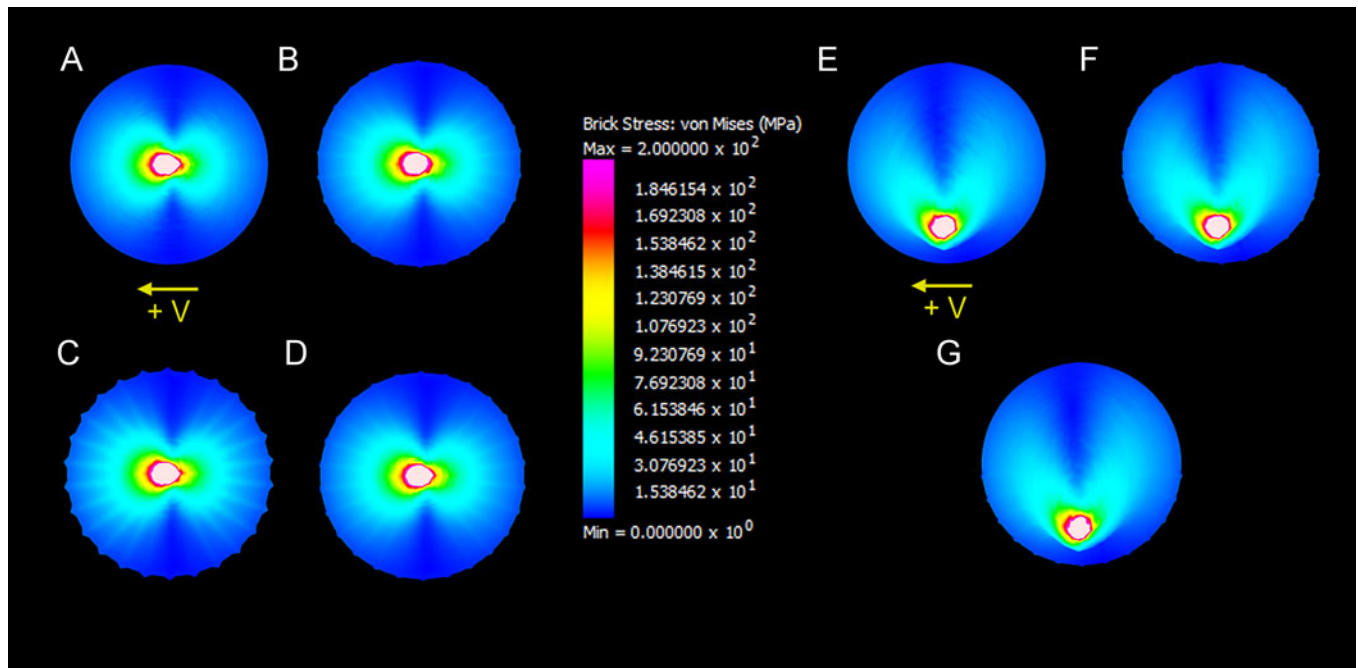
Figure 10. Finite element analysis (FEA) maps for the Bite and Pull load case. Models depict von Mises stress distribution for: A, No Ridges (Conical) model; B, Average Ridges model; C, Large Ridges model; D, Rounded Ridges model; E, No Ridges (Recurved) model; F, Symmetrical Ridges model; G, Lingual Clustering model. All models are shown in occlusal view. Areas of white denote stress higher than 2×10^2. Arrows indicate direction of applied load force on all models. +V indicates vertical load force has been applied on all models.

and although our *Bottosaurus* specimens have not been identified to species level, the comparable morphology suggests an equivalent function. Although purportedly molluscivorous mosasaurs such as *Globidens* and *Carinodens* developed similarly robust and ridged teeth (Schulp 2005), the mosasaurs in this dataset—*Mosasaurus missouriensis* (USNM 4910) and *Tylosaurus proriger* (USNM 3885)—bear a recurved dentition to process meat, such as fish (Konishi et al. 2014), with broad, rounded, and low-relief ridges. The ichthyosaurs are the only group in which lingual clustering is universally absent (Appendix 3). Ichthyosaur ridge morphology is also highly conserved, consisting of dense, parallel, and rounded ridges that extend an equal length along the tooth crown (although the exact length differs between specimens). The few spinosaurid specimens in the dataset present wider, low-relief ridges (Appendix 3), but descriptions of various spinosaurid dentitions suggest a diversity of ridge morphologies (Buffetaut 2013). Odontocetes bear some of the most unique ridge morphologies in the dataset, ranging from discontinuous ridges that present as elongated bumps (USNM 25210 Tooth 2) to basally or exceptionally anastomosed ridges (USNM 25210 Tooth 1; USNM 23546) (Appendix 3). Although some rarer ridge morphologies may be considered potentially taxonomically informative, such as the rugose anastomosis in odontocetes, a majority of basic ridge morphologies occur across many clades. Specific combinations of ridge morphologies, such as low-density, high-relief, and lingually clustered ridges in some pliosaurids (e.g., NHM 2680; NHM 46239 B), may provide more taxonomic information than the individual traits analyzed here, but this is beyond the scope of this paper.

FEA

The similarities between von Mises stress distributions suggest that, overall, models of the same crown shape exhibit no substantial difference in their response to force beside a slightly increased

stress localized within ridges (Figs. 6–10). The otherwise comparable gradient of stress across the crown indicates that apicobasal ridges have little impact on overall tooth crown strength in these models. While, as mentioned, these results cannot account for internal heterogeneity between enamel and dentine material properties, they demonstrate the lack of influence of the ridges' external morphology on stress distribution. Furthermore, the general consistency of stress levels across the range of ridge morphologies implies that ridge shape, size, and arrangement do not contribute to a substantial increase in crown strength. While the mechanical cause of the slightly higher stress within ridges is unclear (although it may be attributable to the smaller surface area), the interjacent smooth enamel shows a rate of vertical stress decrease equal to that of smooth models. This similarity between gradients suggests that the ridges do not act to channel stress away from the crown or alleviate its loading in any form.

The overall Bite distribution patterns recorded in our models (both recurved and conical) resemble those documented in comparably shaped teeth in a recent study (Pollock et al. 2022). Similarly, the bifurcated stress patterns across all teeth in our Shake load case reflect the results under those authors' equivalent Pull load case (Pollock et al. 2022), although the highest concentration of stress occurs closer to the base of their models due to the difference in point loading location. Our results further align with those in a previous study on von Mises stress distributions in smooth snake fangs (Rajabizadeh et al. 2021). When recurved models were subjected to vertical loading (equivalent to the Bite load case), the study documented a similar bifurcation of stress with localization on the lingual face of the crown. A lingual localization of stress also appears on the finite element map of a tooth from the extant shark *Sphyrna mokarran* (Whitenack et al. 2011). Although the crown of *S. mokarran* bears a higher degree of labiolingual compression, its overall curvature resembles that of the three recurved models and is thus potentially subject to

similar forces under longitudinal load cases. As none of the specimens used in these studies bear visible apicobasal ridges, the similarity between distribution patterns suggests that stress distribution is predominantly a product of crown shape rather than the influence of apicobasal ridges.

Relationships between Stress Distribution and Ridge Locations.
The results of the finite element modeling deliver additional insight into the relationships between stress distribution and the position of ridges. If enhanced tooth strength were indeed a significant selective pressure, the centralization of stress upon the apex should lead to a greater need for strength around this region. Apicobasal ridges that increase in prominence toward the apex have been described, but only rarely, such as in the mosasaur *Globidens phosphaticus* (Bardet et al. 2005) or in teeth from *Bottosaurus* (USNM 540758) and *Gavialosuchus* (USNM 244431) in the current dataset. Overall, our morphometrics indicate that the average apicobasal ridge ends at approximately 72% of the height of the tooth crown (Appendix 2). This assessment may even be a slight overestimation, as ridges that ended below the cross section at 50% of the crown height were not able to be included in the sampling pool, and some taxa have developed a number of ridges that disappear beneath this point, including plesiosaurs (NHM 430179; NHM 46239 B), odontocetes (USNM 11962), and crocodilians (USNM 205338). However, as most ridges fail to reach the apex, it is uncertain whether they would increase the second moment of area sufficiently to reduce the chance of buckling.

While the stress concentrations generally do not coincide with the locations of ridges, one exception exists in the recurved tooth shape. McCurry et al. (2019) suggest that the lingual clustering observed in many recurved teeth could act to dissipate stress created along the lingual face as a product of the recurved shape. When subjected to the Bite load case in this study, all recurved models do exhibit a concentration of stress toward the lingual face (Fig. 6E–G). This pattern conflicts with the results of the conical models, which display a uniform decrease of stress under the same Bite load case (Fig. 6A–D). Although this could indicate that apicobasal ridges are lingually clustered in recurved forms to alleviate the increased stress, in congruence with the hypothesis of McCurry et al. (2019), the lack of stress reduction in ridged models alludes to another purpose.

As this study investigated only the most common tooth crown shapes in aquatic-feeding amniotes, future research could be conducted into the relationships between stress distribution and ridge locations on less common tooth shapes. Such shapes may consist of the multicusped form found in several extinct odontocetes, including *Zygorhiza kochii* (USNM 11962) and *Aetiocetus cotylalveus* (USNM 25210 Tooth 1) or the flattened dentition of the crocodilian *Bottosaurus* (USNM 540758).

Evaluating the Strength Hypothesis

The strength hypothesis has been widely referenced in the literature on aquatic-feeding tetrapods (Rieppel and Labhardt 1979; Schulp 2005; Young et al. 2014; Zverkov et al. 2018). However, these claims are based on mechanical theory rather than a quantitative assessment of relevant traits. In *Varanus niloticus*, an extant varanid bearing apicobasal ridges, the dietary transition from insectivory to molluscivory that occurs at adulthood is associated with the appearance of ridges on the tooth crown (Rieppel and Labhardt 1979). This ontogenetic shift has been interpreted

as an adaptation to strengthen the teeth in response to a more durable prey source, with the ridges channeling pressure down the crown's surface (Rieppel and Labhardt 1979). As *V. niloticus* is known to feed predominantly upon aquatic mollusks as well as crabs and amphibians (Dalhuijsen et al. 2014), it is more probable that the ridges evolved to address a challenge in aquatic feeding, such as reduced grip (Chomba and M'Simuko 2013), rather than durophagy—a conclusion that is equally applicable to the taxa studied here.

Alternative Hypotheses of Ridge Function

With the support of previous research (Sander 1999, 2000; McCurry et al. 2019), our results indicate that the improvement of crown strength was unlikely to be a primary function of apicobasal ridges in aquatic-feeding amniotes. Additionally, our findings may shed light on other hypotheses that focus upon the ridges interacting with the prey item, rather than augmenting the crown.

Our data dispute the probability of the puncture hypothesis, which argues that apicobasal ridges may have conferred an advantage in predation by acting as a cutting edge, improving the crown's ability to puncture and quickly entrap prey items (McCurry et al. 2019). While ridges around the apex would provide the most assistance during prey puncture (Vaeth et al. 1985; McCurry et al. 2019), our dataset found that most ridges fail to reach the upper quarter of the crown.

Supporting many past findings (Buffetaut 2013; Richter et al. 2013; Young et al. 2014), a variety of tooth specimens in the current dataset display an increased prominence or clustering of apicobasal ridges on the lingual surface of the crown, including the pliosaurids *Kronosaurus queenslandicus* (KKF 0534) and *Liopleurodon ferox* (NHM 2680), an indeterminate *Spinosaurus* species (ROM 64659), and the crocodilian *Deinosuchus rugosus* (USNM 5351) (Appendix 3). The occurrence of clustering upon the lingual face coincides with the region that contacts maximally with prey items (McCurry et al. 2019). This in turn indicates that ridges may have been adapted primarily for prey interaction (McCurry et al. 2019), as serrated or cutting edges in carnivore teeth are commonly located on areas that contact the substrate to aid in processing (D'Amore 2009).

The array of characteristics benefiting grip efficiency in aquatic feeders, such as spiricules on the toes of sea eagles (Chomba and M'Simuko 2013) and sharp, elongate teeth in sharks (Bergman et al. 2017), implies a substantial selective pressure for enhanced grasping mechanisms in these predators. The evolution of the forelimbs into flippers or flipper-like appendages in many secondarily aquatic taxa restricts these clades to grasping with only their jaws. As such, any adaptation for grip improvement would be localized to the cranial region and, due to its direct contact with prey items, would almost certainly involve the dentition. Previous physical testing on the scales of male sea snakes established that increased rugosity resulted in maximized friction and grip (Avolio et al. 2006). As this aided the male to maintain contact with the female during copulation in the slippery medium of water (Avolio et al. 2006), the addition of apicobasal ridges—particularly rugose morphologies such as in *Squalodon* cheek teeth (USNM 23546)—could equally assist aquatic predators to grip struggling prey items in the same medium. This is further supported by the development of rugose crown apices in some crocodyliform and ichthyosaur taxa (Massare 1987; Fischer et al. 2011), which may demonstrate a selection for convergent grip morphologies in areas without ridges.

However, a function in prey handling does not parsimoniously account for ridge configurations that remain symmetrical across the entire crown circumference. Such configurations may instead provide evidence for the removal hypothesis, which proposes that apicobasal ridges functioned like anti-stick grooves in a knife, reducing suction to allow the removal of prey caught in the teeth (McCurry et al. 2019). Wright et al. (1979) argued that the need for removal efficiency would be greater on the mesial face of the tooth due to its initial contact with prey, which would provide an advantage in ridges evolving on regions of the tooth with reduced prey contact in comparison to the lingual surface.

Conclusions

This study finds that within typical aquatic-feeding amniote dentition, external apicobasal ridges appear to have little impact upon the ability of the tooth to resist biologically relevant loading. The overall distributions of von Mises stress in finite element maps are highly similar between smooth and ridged tooth crown models of identical shape, differing only in a slightly increased stress localized within ridges, while retaining an equal rate of decreasing stress on areas of smooth enamel. These parallel gradients suggest that the higher-stress ridges do not alleviate crown stress. Furthermore, this trend of similarity persists across all tested ridge morphologies, demonstrating that variation in ridge size, shape, and arrangement around the crown is unlikely to influence the tooth's resistance to failure.

The factors shaping tooth morphology may be related to the selective pressures imposed by predation, such as the need for increased grip on slippery prey, as the variance in intra-taxon ridge morphology supports previous hypotheses that dental ornamentation is more affected by the functional requirements of diet than by phylogenetic grouping.

Our results offer a foundation for future research into other prominent hypotheses of apicobasal ridge function, including improved removal efficiency and enhanced grip. Although our data on tooth crown and ridge morphometrics indicate varying support for these hypotheses across the range of ridge morphologies, further testing is required to explore their biomechanical nuances and return quantifiable evidence. Nevertheless, the absence of stress resistance in our models and the prevalence of lingual clustering in fossil specimens supports the concept that apicobasal ridges evolved for direct contact with prey items, rather than to augment crown robustness.

Literature Cited

Araújo, R., and M. J. Polcyn. 2013. A biomechanical analysis of the skull and adductor chamber muscles in the Late Cretaceous plesiosaur *Libonectes*. *Palaeontologia Electronica* **16**:10A.

Avolio, C., R. Shine, and A. J. Pile. 2006. The adaptive significance of sexually dimorphic scale rugosity in sea snakes. *American Naturalist* **167**: 728–738.

Bardet, N., X. Pereda Suberbiola, M. Iarochène, M. Amalik, and B. Bouya. 2005. Durophagous Mosasauridae (Squamata) from the Upper Cretaceous phosphates of Morocco, with the description of a new species of *Globidens*. *Netherlands Journal of Geosciences* **84**:167–175.

Benson, R. B. J., E. M. G. Fitzgerald, T. H. Rich, and P. Vickers-Rich. 2013. Large freshwater plesiosaurian from the Cretaceous (Aptian) of Australia. *Alcheringa* **37**:456–461.

Bensonne, L. M., E. F. Bodereau, G. Cabanillas, and A. Dominguez. 2014. Analysis of biomechanical behaviour of anterior teeth using two different methods: finite element method and experimental tests. *Engineering* **6**:148–158.

Bergman, J. N., M. J. Lajeunesse, and P. J. Motta. 2017. Teeth penetration force of the tiger shark *Galeocerdo cuvier* and sandbar shark *Carcharhinus plumbeus*. *Journal of Fish Biology* **91**:460–472.

Bourke, J., S. Wroe, K. Moreno, C. McHenry, and P. Clausen. 2008. Effects of gape and tooth position on bite force and skull stress in the dingo (*Canis lupus dingo*) using a 3-dimensional finite element approach. *PLoS ONE* **3**: e2200.

Braun, J., and W. E. Reif. 1985. A survey of aquatic locomotion in fishes and tetrapods. *Neues Jahrbuch für Geologie und Paläontologie, Abhandlungen* **169**:307–332.

Buffetaut, E. 2013. An early spinosaurid dinosaur from the Late Jurassic of Tendaguru (Tanzania) and the evolution of the spinosaurid dentition. *Oryctos* **10**:1–8.

Chomba, C., and E. M'Simuko. 2013. Nesting patterns of raptors; White backed vulture (*Gyps africanus*) and African fish eagle (*Haliaeetus vocifer*), in Lochinvar National Park on the kafue flats, Zambia. *Open Journal of Ecology* **3**:325–330.

Chun, K. J., H. H. Choi, and J. Y. Lee. 2014. Comparison of mechanical property and role between enamel and dentin in the human teeth. *Journal of Dental Biomechanics* **5**:1758736014520809.

Ciampaglio, C. N., G. A. Wray, and B. H. Corliss. 2005. Convergence in tooth morphology among marine Mesozoic–Cenozoic sharks, reptiles, and mammals. *Sedimentary Record* **3**:4–8.

Clough, R. W. 1990. Original formulation of the finite element method. *Finite Elements in Analysis and Design* **7**:89–101.

Cohen, K. E., H. I. Weller, and A. P. Summers. 2020. Not your father's homodonty—stress, tooth shape, and the functional homodont. *Journal of Anatomy* **237**:837–848.

Cossette, A. P., and C. A. Brochu. 2018. A new specimen of the alligatoroid *Bottosaurus harlani* and the early history of character evolution in alligatorids. *Journal of Vertebrate Palaeontology* **38**:e1486321.

Crofts, S. B., S. M. Smith, and P. S. L. Anderson. 2020. Beyond description: the many facets of dental biomechanics. *Integrative and Comparative Biology* **60**:594–607.

Dalhuijsen, K., W. R. Branch, and G. J. Alexander. 2014. A comparative analysis of the diets of *Varanus albigularis* and *Varanus niloticus* in South Africa. *African Zoology* **49**:83–93.

D'Amore, D. C. 2009. A functional explanation for denticulation in theropod dinosaur teeth. *Anatomical Record* **292**:1297–1314.

Dumont, E. R., J. Piccirillo, and I. R. Grosse. 2005. Finite-element analysis of biting behavior and bone stress in the facial skeletons of bats. *Anatomical Record, part A* **283A**:319–330.

Dumont, E. R., I. R. Grosse, and G. J. Slater. 2009. Requirements for comparing the performance of finite element models of biological structures. *Journal of Theoretical Biology* **256**:96–103.

Erickson, G. M., P. M. Gignac, S. J. Steppan, A. K. Lappin, K. A. Vliet, J. D. Brueggen, B. D. Inouye, D. Kledzik, and G. J. Webb. 2012. Insights into the ecology and evolutionary success of crocodilians revealed through bite-force and tooth-pressure experimentation. *PLoS ONE* **7**:e31781.

Fischer, V., A. Clément, M. Guiomar, and P. Godefroit. 2011. The first definite record of a Valanginian ichthyosaur and its implications on the evolution of post-Liassic Ichthyosauria. *Cretaceous Research* **32**:155–163.

Fischer, V., M. S. Arkhangelsky, I. M. Stenshin, G. N. Uspensky, N. G. Zverkov, and R. B. J. Benson. 2015. Peculiar macrophagous adaptations in a new Cretaceous pliosaurid. *Royal Society Open Science* **2**:150552.

Fischer, V., R. F. Bennion, D. Foffa, J. A. MacLaren, M. R. McCurry, K. M. Melstrom, and N. Bardet. 2022. Ecological signal in the size and shape of marine amniote teeth. *Proceedings of the Royal Society of London B* 289:20221214.

Fish, F. E. 2016. Secondary evolution of aquatic propulsion in higher vertebrates: validation and prospect. *Integrative and Comparative Biology* 56:1285–1297.

Gallagher, A. J., Y. P. Papastamatiou, and A. Barnett. 2018. Apex predatory sharks and crocodiles simultaneously scavenge a whale carcass. *Journal of Ethology* 36:205–209.

Hendrickx, C., O. Mateus, and R. Araújo. 2015. A proposed terminology of theropod teeth (Dinosauria, Saurischia). *Journal of Vertebrate Paleontology* 35:e982797.

Herbst, E. C., S. Lautenschlager, D. Bastiaans, F. Miedema, and T. M. Scheyer. 2021. Modeling tooth enamel in FEA comparisons of skulls: comparing common simplifications with biologically realistic models. *iScience* 24:103182.

Houssaye, A., and F. E. Fish. 2016. Functional (secondary) adaptation to an aquatic life in vertebrates: an introduction to the symposium. *Integrative and Comparative Biology* 56:1266–1270.

Howell, A. B. 1930. *Aquatic mammals: their adaptions to life in the water*. CC Thomas, Springfield, Ill.

Jansen van Vuuren, L., J. A. Kieser, M. Dickenson, K. C. Gordon, and S. J. Fraser-Miller. 2016. Chemical and mechanical properties of snake fangs. *Journal of Raman Spectroscopy* 47:787–795.

Khalid, Y. A., C. L. Chan, B. B. Sahari, and A. M. S. Hamouda. 2004. Bending behaviour of corrugated web beams. *Journal of Materials Processing Technology* 150:242–254.

Koc, D., A. Dogan, and B. Bek. 2010. Bite force and influential factors on bite force measurements: a literature review. *European Journal of Dentistry* 4:223–232.

Konishi, T., M. G. Newbrey, and M. W. Caldwell. 2014. A small, exquisitely preserved specimen of *Mosasaurus missouriensis* (Squamata, Mosasauridae) from the upper Campanian of the Bearpaw Formation, western Canada, and the first stomach contents for the genus. *Journal of Vertebrate Paleontology* 34:802–819.

Lukeneder, A., and N. Zverkov. 2020. First evidence of a conical-toothed pliosaurid (Reptilia, Sauropterygia) in the Hauterivian of the Northern Calcareous Alps, Austria. *Cretaceous Research* 106:104248.

Madzia, D. 2016. A reappraisal of *Polyptychodon* (Plesiosauria) from the Cretaceous of England. *PeerJ* 4:e1998.

Massare, J. A. 1987. Tooth morphology and prey preference of Mesozoic marine reptiles. *Journal of Vertebrate Paleontology* 7:121–137.

Maxwell, E. E., M. W. Caldwell, and D. O. Lamoureux. 2012. Tooth histology, attachment, and replacement in the Ichthyopterygia reviewed in an evolutionary context. *Paläontologische Zeitschrift* 86:1–14.

McCurry, M. R., A. R. Evans, E. M. G. Fitzgerald, C. R. McHenry, J. Bevitt, and N. D. Pyenson. 2019. The repeated evolution of dental apicobasal ridges in aquatic-feeding mammals and reptiles. *Biological Journal of the Linnean Society* 127:245–259.

McNeel, R. 2019. *Rhinoceros*. Robert McNeel & Associates, Seattle, Wash. https://www.mcneel.com.

Milewski, G. 2005. Numerical and experimental analysis of effort of human tooth hard tissues in terms of proper occlusal loadings. *Acta of Bioengineering and Biomechanics* 7:47–59.

Neves, A. A., Coutinho, E., Alves, H. D. L., and J. T. de Assis. 2015. Stress and strain distribution in demineralized enamel: a micro-CT based finite element study. *Microscopy Research and Technique* 78:865–872.

Palci, A., A. R. H. LeBlanc, O. Panagiotopoulou, S. G. C. Cleuren, H. M. Abraha, M. N. Hutchinson, A. R. Evans, M. W. Caldwell, and M. S. Y. Lee. 2021. Plicidentine and the repeated origins of snake venom fangs. *Proceedings of the Royal Society of London B* 288:20211391.

Pollock, T. I., O. Panagiotopoulou, D. P. Hocking, and A. R. Evans. 2022. Taking a stab at modelling canine tooth biomechanics in mammalian carnivores with beam theory and finite-element analysis. *Royal Society Open Science* 9:220701.

Preuschoft, H., W. E. Reif, and W. H. Müller. 1974. Funktionsanpassungen in form und struktur an haifischzähnen. *Zeitschrift für Anatomie und Entwicklungsgeschichte* 143:315–344.

Rajabizadeh, M., S. Van Wassenbergh, C. Mallet, M. Rücklin, and A. Herrel. 2021. Tooth-shape adaptations in aglyphous colubrid snakes inferred from three-dimensional geometric morphometrics and finite element analysis. *Zoological Journal of the Linnean Society* 191:454–467.

R Core Team. 2021. *R: a language and environment for statistical computing*. R Foundation for Statistical Computing, Vienna, Austria. https://www.R-project.org.

Richter, U., A. Mudroch, and L. G. Buckley. 2013. Isolated theropod teeth from the Kem Kem beds (early Cenomanian) near Taouz, Morocco. *Paläontologische Zeitschrift* 87:291–309.

Rieppel, O., and L. Labhardt. 1979. Mandibular mechanics in *Varanus niloticus* (Reptilia: Lacertilia). *Herpetologica* 35:158–163.

Sander, P. M. 1999. The microstructure of reptilian tooth enamel: terminology, function, and phylogeny. *Münchner Geowissenschaftliche Abhandlungen* 38:1–102.

Sander, P. M. 2000. Prismless enamel in amniotes: terminology, function and evolution. Pp. 92–106 *in* M. F. Teaford, M. M. Smith, and M. W. J. Ferguson, eds. *Development, function and evolution of teeth*. Cambridge University Press, Cambridge.

Schulp, A. S. 2005. Feeding the mechanical mosasaur: what did *Carinodens* eat? *Netherlands Journal of Geosciences* 84:345–357.

Sulcova, M. L., O. Zahradnicek, J. Dumkova, H. Dosedelova, J. Krivanek, M. Hampl, M. Kavkova, et al. 2020. Developmental mechanisms driving complex tooth shape in reptiles. *Developmental Dynamics* 249:441–464.

Taylor, M. A. 1992. Functional anatomy of the head of the large aquatic predator *Rhomaleosaurus zetlandicus* (Plesiosauria, Reptilia) from the Toarcian (Lower Jurassic) of Yorkshire, England. *Philosophical Transactions of the Royal Society of London B* 335:247–280.

Thewissen, J., and S. Nummela. 2008. Introduction: on becoming aquatic. Pp. 1–25 *in* J. Thewissen and S. Nummela, eds. *Sensory evolution on the threshold: adaptations in secondarily aquatic vertebrates*. University of California Press, Berkeley.

Vaeth, R. H., D. A. Rossman, and W. Shoop. 1985. Observations of tooth surface morphology in snakes. *Journal of Herpetology* 19:20–26.

Whitenack, L. B., D. C. Simkins Jr., and P. J. Motta. 2011. Biology meets engineering: the structural mechanics of fossil and extant shark teeth. *Journal of Morphology* 272:169–179.

Wright, D. L., K. V. Kardong, and D. L. Bentley. 1979. The functional anatomy of the teeth of the western terrestrial garter snake, *Thamnophis elegans*. *Herpetologica* 35:223–228.

Young, B. A., and K. V. Kardong. 1996. Dentitional surface features in snakes (Reptilia: Serpentes). *Amphibia-Reptilia* 17:261–276.

Young, M. T., L. Steel, S. L. Brusatte, D. Foffa, and Y. Lepage. 2014. Tooth serration morphologies in the genus *Machimosaurus* (Crocodylomorpha, Thalattosuchia) from the Late Jurassic of Europe. *Royal Society Open Science* 1:140269.

Zverkov, N. G., V. Fischer, D. Madzia, and R. B. J. Benson. 2018. Increased pliosaurid dental disparity across the Jurassic–Cretaceous transition. *Palaeontology* 61:825–846.

Appendix 1. Specimen List

List of isolated tooth specimens in the six major aquatic-feeding amniote clades measured for this study. Specimens are grouped by taxa.

Specimen no.	Group	Genus or species
USNM 508536	Crocodylia	*Bottosaurus* sp.
USNM 540758	Crocodylia	*Bottosaurus* sp.
USNM 5351	Crocodylia	*Deinosuchus rugosus*
USNM 299794	Crocodylia	*Gavialosuchus americanus*
USNM 244431	Crocodylia	*Gavialosuchus* sp.
USNM 16115	Crocodylia	*Goniopholis crassidens*
USNM 11823	Crocodylia	Indet.
USNM 356035	Crocodylia	Indet.
USNM 358831	Crocodylia	Indet.
USNM 25243 RED	Crocodylia	Indet.
USNM 205338	Crocodylia	*Purussaurus* sp.
ROM 1860	Ichthyosauria	*Ichthyosaurus communis*
ROM 12810 Tooth A	Ichthyosauria	*Ichthyosaurus* sp.
USNM 412523 Large	Ichthyosauria	Indet.
USNM 412523 Small	Ichthyosauria	Indet.
ROM 12809 Tooth A	Ichthyosauria	Indet.
ROM 12809 Tooth B	Ichthyosauria	Indet.
ROM 12809 Tooth C	Ichthyosauria	Indet.
ROM 12809 Tooth D	Ichthyosauria	Indet.
ROM 12809 Tooth E	Ichthyosauria	Indet.
ROM 12809 Tooth F	Ichthyosauria	Indet.
ROM 00334 A	Ichthyosauria	*Pervushovisaurus campylodon*
USNM 4910	Mosasauridae	*Mosasaurus missouriensis*
USNM 3885	Mosasauridae	*Tylosaurus proriger*
USNM 25210 Tooth 1	Odontoceti	*Aetiocetus cotylalveus*
USNM 25210 Tooth 2	Odontoceti	*Aetiocetus cotylalveus*
USNM 23546	Odontoceti	*Squalodon calvertensis*
USNM 25711	Odontoceti	*Squalodon* sp.
USNM 11962	Odontoceti	*Zygorhiza kochii*
NHM 10929	Plesiosauria	Indet.
ROM 71030	Plesiosauria	Indet.
ROM 71290 B	Plesiosauria	Indet.
NHM 430719	Plesiosauria	Indet.
ROM 71033	Plesiosauria	Indet.
KKF 0534	Plesiosauria	*Kronosaurus queenslandicus*
KKF Shaw	Plesiosauria	*Kronosaurus queenslandicus*
NHM 2680	Plesiosauria	*Liopleurodon ferox*
ROM 5596	Plesiosauria	*Pliosaurus brachydeirus*
USNM 25444	Plesiosauria	*Pliosaurus grandis*
NHM 5796	Plesiosauria	*Pliosaurus* sp.

(*Continued*)

Appendix 1. (*Continued.*)

Specimen no.	Group	Genus or species
NHM 46239 B	Plesiosauria	*Pliosaurus* sp.
USNM 16153 B	Plesiosauria	*Polyptychodon interruptus*
NHM 43171	Plesiosauria	*Polyptychodon interruptus*
ROM 1872 A	Plesiosauria	*Polyptychodon interruptus*
ROM 1872 B	Plesiosauria	*Polyptychodon interruptus*
NHM 1325	Plesiosauria	*Rhomaleosaurus* sp.
ROM 64659	Spinosauridae	*Spinosaurus* sp.
ROM 65992	Spinosauridae	*Spinosaurus* sp.

Appendix 2. Tooth Crown Data

Tooth crown measurements for all tooth specimens. Specimens labeled "Anastomosed" had anastomosed ridges that were impractical to measure for individual length. Specimens labeled "Discontinuous" had discontinuous ridge "patches" that could not be accurately measured for length along the tooth. Specimens labeled "Indet." were mold or cast fossils for which one or more faces were obstructed.

Specimen no.	Average ridge % up crown height	Crown height (mm)	Crown width mesial/distal (mm)	Crown width lingual/buccal (mm)
USNM 508536	Anastomosed	14.68	12.99	10.37
USNM 540758	92	8.07	15.48	7.68
USNM 5351	62.5	36.09	23.53	24.06
USNM 299794	71.5	50.8	22.67	20.43
USNM 244431	Discontinuous	64.51	35.96	33.19
USNM 16115	81	24.01	13.87	11.93
USNM 11823	Anastomosed	34.34	20.14	20.24
USNM 356035	84.5	25.55	8.47	8.79
USNM 358831	89.5	17.2	11.24	11.57
USNM 25243 RED	77	34.3	16.15	15.35
USNM 205338	62.5	73.88	46.55	41.35
ROM 1860	79	12.21	9.48	9.03
ROM 12810 Tooth A	80	22.9	4.16	Indet.
USNM 412523 Large	79	17.14	15.91	13.35
USNM 412523 Small	76.5	17.36	11.08	10.69
ROM 12809 Tooth A	68	18.28	11.41	Indet.
ROM 12809 Tooth B	77.5	19.24	13.46	Indet.
ROM 12809 Tooth C	90	11.86	7.22	Indet.
ROM 12809 Tooth D	72.5	12.43	7.94	Indet.
ROM 12809 Tooth E	78.5	13.56	10.07	Indet.
ROM 12809 Tooth F	90.5	13.4	8.38	Indet.
ROM 00334 A	83.5	22.32	12.67	12.53
USNM 4910	59	36.12	24.81	18.28
USNM 3885	65	36.4	28.57	28.56
USNM 25210 Tooth 1	61.5	12	8.95	5.8
USNM 25210 Tooth 2	Discontinuous	7.56	9.21	5.84
USNM 23546	Anastomosed	25.99	26.43	12.91
USNM 25711	68	21.41	15.17	8.58
USNM 11962	56.5	44.68	38.11	15.34
NHM 10929	73.5	18.2	4.49	Indet.
ROM 71030	64.5	42.24	10.86	10.04
ROM 71290 B	57	14.4	7.62	9.37
NHM 430719	75	48.81	27.49	25.08
ROM 71033	82.5	23.33	10.52	11.41
KKF 0534	67.5	68.82	35.28	33.69
KKF Shaw	75.5	67	24.08	33.83
NHM 2680	77.5	39.46	20.48	19.17
ROM 5596	65	59.99	32.35	33.92

(*Continued*)

Appendix 2. (*Continued.*)

Specimen no.	Average ridge % up crown height	Crown height (mm)	Crown width mesial/distal (mm)	Crown width lingual/buccal (mm)
USNM 25444	60	65	22.51	16.16
NHM 5796	81.5	41.19	23.73	20.81
NHM 46239 B	75	59	35.43	33.42
USNM 16153 B	69	57.14	27.99	24.71
NHM 43171	66	17.65	11.05	10.72
ROM 1872 A	85	22.01	14.27	12.25
ROM 1872 B	77	33.98	19.77	18.64
NHM 1325	73.5	29.52	12.03	Indet.
ROM 64659	63	53.16	29.45	28.85
ROM 65992	54.5	26.71	11.01	10.81

Appendix 3. Apicobasal Ridge Data

Apicobasal measurements and morphological data for all tooth specimens. All data were drawn from a cross section at 50% of the visible tooth height. Specimens were excluded from the overall average of ridge measurements if fewer than 10 ridges were recorded at the cross section. Specimens labeled "Indet." were mold or cast fossils for which one or more faces were obstructed. Ridge counts for these specimens are also potential underestimations, as only visible ridges were counted to avoid exaggeration. Specimens with no measurements recorded bore ridges that ended below the cross section.

Specimen no.	Average ridge width (mm)	Average ridge height (mm)	Ridge count	Lingual clustering
USNM 508536	0.196	0.016	16	No
USNM 540758	0.371	0.079	61	No
USNM 5351	0.601	0.112	30	Yes
USNM 299794	1.718	0.158	18	No
USNM 244431	0	0	0	No
USNM 16115	0.457	0.053	34	No
USNM 11823	0.615	0.19	60	No
USNM 356035	0.41	0.036	28	Yes
USNM 358831	0.382	0.059	61	No
USNM 25243 RED	0.784	0.052	18	No
USNM 205338	0.819	0.071	11	No
ROM 1860	0.437	0.128	25	No
ROM 12810 Tooth A	0.635	0.08	2	Indet.
USNM 412523 Large	0.447	0.031	60	No
USNM 412523 Small	0.509	0.05	42	No
ROM 12809 Tooth A	0.448	0.065	8	Indet.
ROM 12809 Tooth B	1.374	0.154	10	Indet.
ROM 12809 Tooth C	0.445	0.055	2	Indet.
ROM 12809 Tooth D	0.28	0.05	4	Indet.
ROM 12809 Tooth E	0.429	0.101	12	Indet.
ROM 12809 Tooth F	0.432	0.063	12	Indet.
ROM 00334 A	0.492	0.083	44	No
USNM 4910	1.343	0.091	19	Yes

(*Continued*)

Appendix 3. (*Continued.*)

Specimen no.	Average ridge width (mm)	Average ridge height (mm)	Ridge count	Lingual clustering
USNM 3885	1.2	0.098	22	No
USNM 25210 Tooth 1	0.404	0.137	11	Yes
USNM 25210 Tooth 2	0.363	0.061	7	Yes
USNM 23546	0.383	0.134	57	Yes
USNM 25711	0.782	0.079	10	No
USNM 11962	0.61	0.126	28	Yes
NHM 10929	0.329	0.064	12	Indet.
ROM 71030	0.134	0.014	70	Yes
ROM 71290 B	0.278	0.023	16	Yes
NHM 430719	0.809	0.351	11	Yes
ROM 71033	0.208	0.015	63	Yes
KKF 0534	0.839	0.239	42	Yes
KKF Shaw	1.052	0.158	29	Yes
NHM 2680	0.771	0.342	18	Yes
ROM 5596	1.275	0.554	15	Yes
USNM 25444	0.933	0.352	14	Yes
NHM 5796	0.472	0.104	37	No
NHM 46239 B	1.08	0.469	11	Yes
USNM 16153 B	0.77	0.192	38	Yes
NHM 43171	0.643	0.123	14	No
ROM 1872 A	0.535	0.22	45	No
ROM 1872 B	0.732	0.172	29	Yes
NHM 1325	0.366	0.081	15	Indet.
ROM 64659	0.991	0.108	29	Yes
ROM 65992	0.42	0.048	24	Yes